DOI: 10.1002/ejic.200900453

Silver Nanofibres by a Novel Electrospinning Process: Nanofibres with Plasmon Resonance in the IR Region and Thermal Hysteresis Electrical Conductivity Features

Nasser A. M. Barakat,*[a,b] Taha E. Farrag,[a] Muzafar A. Kanjwal,[c] Soo-Jin Park,[b] Faheem A. Sheikh,[d] and Hak Yong Kim*[e]

Keywords: Silver / Nanostructures / Electrospinning of colloidal solutions / Surface plasmon resonance / Electrochemistry

In this study, we have introduced electrospinning of a colloidal solution rather than the conventional sol–gel process as a novel strategy to produce silver nanofibres. Typically, a silver acetate/polyvinyl alcohol colloidal solution was successfully electrospun. Electrophoretic light scattering (ELS) and dynamic light scattering (DLS) analyses have affirmed that the electrospun solution is a colloid with a ζ-potential of –2 mV and average particle diameter of 373 ± 1 nm. Moreover, FTIR analysis affirmed that neither the polymer nor silver acetate nanoparticles were affected during the electrospinning process. Calcination of the electrospun mats at 700 °C in an argon atmosphere produced smooth and unbroken pure silver nanofibres. Surface plasmon resonance of the resultant silver nanofibres was detected at 962 nm which is biologically beneficial. Furthermore, the synthesised silver nanofibres revealed thermal hysteresis in the electrical conductivity properties. These advantageous physical features strongly suggest utilising the prepared nanofibres in various fields.

Introduction

The simplicity of the electrospinning process, the diversity of the electrospinnable materials and the unique features of the obtained electrospun nanofibres have generated special interest in both the technique and resultant products.[1–3] The past decades have witnessed tremendous progress in the development of the electrospinning technique for widening the applications of the obtained products. However, many technical issues still need to be resolved before the electrospinning process becomes more popular and the electrospun nanofibres have sufficient strength for industrial level applications. Some researchers have reported modifications of this technique to enhance the alignment of the produced nanofibres.[4,5] Others have focused on the morphology of the obtained nanofibres and they have improved the technique to produce nanofibres with special features.[6–9] In all the previous studies, the researchers have either modified the electrospinning instrumental design or specially treated the resultant product.

Generally, all the reported electrospinning studies have been based on sol–gels. The distinct feature of this solution method is that the precursor should be soluble in a suitable solvent since it has to hydrolyse and polycondensate in the final precursor/polymer mixture to form the gel network. Actually, using only the sol–gel process strongly fettered the applications of the electrospinning process. In this study, we introduced electrospinning of a colloidal solution as a new strategy to broaden the category of the electrospinnable materials. Silver acetate, which is water insoluble, was mixed with aqueous polyvinyl alcohol to form a colloidal mixture which was successfully electrospun. The obtained nanofibre mats were used to produce silver nanofibres which might have wide applications due to the advantages of the nanofibrous shape and the recently discovered distinct features of the noble metal nanostructures.

Noble metal nanostructures such as those based on silver and gold have gained great interest because of their superior electrical, optical, mechanical and catalytic properties.[10–13] Surface plasmon resonance (SPR) is one of the most interesting features of these metal nanoparticles (NPs). SPR is a phenomenon which occurs when light is reflected off thin metal films or NPs. A fraction of the light energy incident at a sharply defined angle can interact with the delocalised electrons in the metal surface (plasmon) thus reducing the

[a] Chemical Engineering Department, Faculty of Engineering, El-Minia University,
El-Minia, Egypt
E-mail: nasbarakat@yahoo.com
[b] Center for Healthcare Technology Development, Chonbuk National University,
Jeonju 561-756, Republic of Korea
[c] Department of Polymer Nano Science and Technology, Chonbuk National University,
Jeonju 561-756, Republic of Korea
[d] Bionano System Engineering Chonbuk National University,
Jeonju 561-756, Republic of Korea
[e] Department of Textile Engineering, Chonbuk National University,
Jeonju 561-756, Republic of Korea
Fax: +82-63 270 2348
E-mail: khy@chonbuk.ac.kr

reflected light intensity.[14] In particular, silver and gold metals are the most popular materials used in this field.[15] However because of its d-s band gap in the UV region,[16] and the smooth effect on the plasmon mode compared with gold,[17] silver is most commonly utilised. Many applications based on SPR have been reported, including medical diagnostics and therapeutics,[18] chemical and biochemical sensors,[19,20] substrates for enhanced spectroscopy[21,22] and light transmission at the sub-wavelength region.[23]

It has been recently reported that the SPR character of the noble metals is closely related to the geometry of the nanoparticles.[14,24] Both calculations and experiments proved that one-dimensional (1D) metal NPs reveal a much greater local field enhancement and therefore more significant applications.[25] Moreover, the relative axial ratio of the 1D nanostructure has considerable impact.[26–28] In general, the longer nanorods exhibit plasmon resonances in the near-infrared (near-IR) region along with high sensitivity. Tunability of the plasmon resonance wavelength in the near-IR region, where human tissue has the highest transmission (i.e. the biological water window), is strongly desirable.[29] Therefore, many reports have presented the production of silver nanorods or nanoparticulate composites with tunability in the near-IR region.[30–33] Among all 1D nanostructures, nanofibres possess the maximum axial ratio, so the prepared silver nanofibres in this study revealed SPR at a wavelength in the IR region (962 nm). Generally, the nanofibrous shape enhances the physical properties. Therefore, the introduced silver nanofibres are expected to have distinct features compared with nanoparticles.

Results and Discussion

The electrospinning technique involves the use of a high voltage to charge the surface of a polymer solution droplet and thus to induce the ejection of a liquid jet through a spinneret. Due to bending instability, the jet is subsequently stretched by many times to form continuous, ultrathin fibres. Therefore, the process is carried out for highly electrically conductive solutions. Consequently, electrospinning is a perfect process for production of many pristine polymeric nanofibres. Moreover, many reports discussed production of metal oxide/composite nanofibres from metal base polymeric electrospun nanofibre mats obtained from electrospinning of sol–gel solutions. In the same fashion, the technique has been exploited to prepare some metal nanofibres.[34,35]

Silver acetate (AgOAc) is not soluble in water and many other common solvents. Accordingly, mixing AgOAc powder with aqueous polyvinyl alcohol (PVA) produces a colloidal solution. The obtained solution is yellowish in colour but stable (i.e. there is no precipitation in the syringe during the electrospinning). To precisely investigate the characteristics of the prepared colloidal solution, measurement of the average hydrodynamic diameter and the particle size distribution were performed using DLS analysis. Figure 1 demonstrates the particle size distribution obtained. As shown in this figure, many particles (≈ 26%) have a very small size (less than 50 nm). The average diameter of the AgOAc particles in the utilised colloidal solution was determined to be 273 ± 1 nm. The zeta (ζ) potential is the most commonly measured parameter characterising colloidal solutions.[36] For a AgOAc/PVA colloidal solution, the measured ζ potential was –2 mV. Figure 2 shows the SEM and FESEM images of the blank PVA and AgOAc/PVA dried nanofibre mats. As shown in part A of Figure 2, which reveals the nanofibres obtained from the pristine PVA, this polymer can be electrospun to produce nanofibres of well defined morphology as there are no beads or agglomerated nanofibres observed in the obtained mats Figure 2 (B) demonstrates the SEM images of the dried AgOAc/PVA nanofibre mats. The electrospinning process of the prepared colloid resulted in relatively smooth nanofibres and addition of the AgOAc particles did not affect the nanofibrous morphology as shown in the figure. Figure 2 (C) represents the FESEM image of the AgOAc/PVA mixture. As can be seen in this figure, smooth and nanofibres of well defined morphology with a wide diameter range were obtained. Close scrutiny of Figure 2 (C) enables observation of some of the silver acetate nanoparticles. These nanoparticles are very few and so small in size so we can say the majority of the silver acetate nanoparticles are trapped inside the PVA nanofibres. As shown in Figure 1, many of the AgOAc particles have small sizes. Moreover, the pristine PVA electrospun mat does not contain any particles, as shown in Figure 2 (A). Therefore, the apparent particles in Figure 2 (C) can be confidently identified as AgOAc.

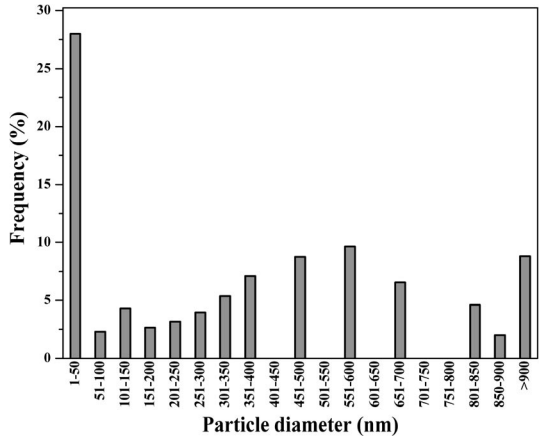

Figure 1. Silver acetate particles size distribution in PVA solution according to DLS analysis.

To confirm that the AgOAc particles had not reacted or hydrolysed during or after the electrospinning process, FTIR analysis was carried out. It is worth mentioning that according to the composition of the colloidal solution used and the molecular weights of AgOAc and PVA, the molar ratio of the hydroxy to the acetate groups in the mixture is almost 52:1. Therefore, if any reaction takes place between these two groups, acetate anions will completely disappear

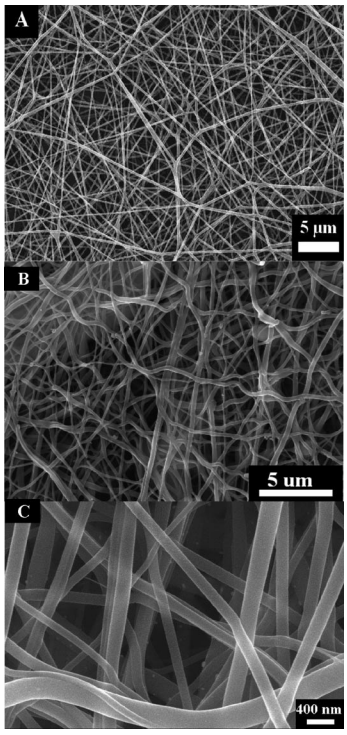

Figure 2. Scanning electron microscope (SEM) images for the dried nanofibre mats of the pristine PVA (A) and silver acetate/PVA (B), and field emission electron microscope (FE SEM) image for silver acetate/PVA nanofibre mats.

from the mixture. Moreover, if the acetate anions hydrolyse in the solution, this will lead to formation of acetic acid which will evaporate during the drying step. Figure 3 shows the FTIR results for the utilised silver acetate, the pristine PVA and the electrospun nanofibre mats. As shown in this figure, the characteristics absorption bands of the acetate anion which appear from 1590–600 cm^{-1} [37,38] can be observed in the spectra of AgOAc and the nanofibre mats. Within this range, two main peaks at 1570 and 1408 cm^{-1} can be clearly seen in the nanofibre mats and the pure AgOAc spectra. No similar peaks at the same wavenumbers can be observed in the pristine PVA spectra. Moreover, all the other small peaks denoting the acetate group can be observed in the electrospun mat spectra. Furthermore, the main molecular structure of PVA was not affected since all the peaks of PVA exist in the electrospun mat spectra. These results indicate that AgOAc particles in the electrospun colloidal solution were not affected and the obtained electrospun PVA nanofibres are trapped the AgOAc particles.

Calcination of the obtained nanofibre mats in an argon atmosphere at 700 °C did not strongly affect the nanofibrous morphology. Figure 4 shows the SEM and FESEM images of the obtained powder after the calcination process. FESEM of the final powder obtained is shown in Figure 4 (the lowest panel). As shown in this figure, the surface morphology of the obtained nanofibres is acceptable and the average diameter of the obtained nanofibres was about 250 nm. However, the calcination temperature affected the

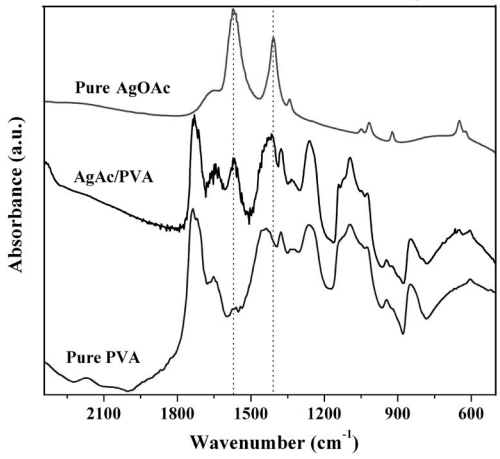

Figure 3. FTIR spectra for pure silver acetate, pristine PVA and silver acetate/PVA electrospun nanofibre mats; the dashed lines demonstrate the locations of the peaks representing the acetate ion.

final morphology and we have performed calcination at three temperatures, namely 500, 700 and 850 °C; 700 °C gave the best morphology.

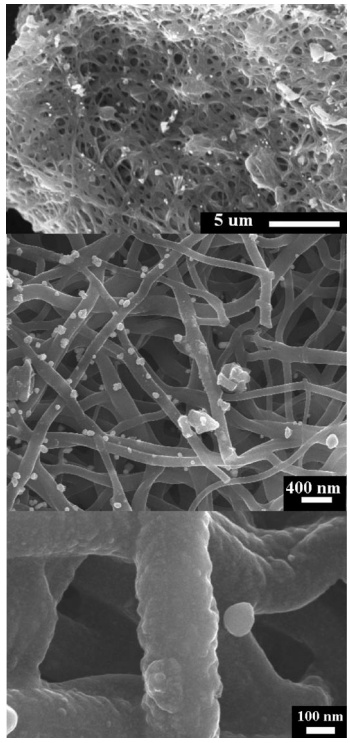

Figure 4. Scanning electron microscope (SEM) and field emission electron microscope (FE SEM) images for silver acetate/PVA nanofibre mats after calcination in an Ar atmosphere at 700 °C.

The polymer is an essential constituent for achieving the electrospinning process. PVA does have wide utilisation in producing metallic nanofibres by the electrospinning methodology because of its novel chemical and thermal characteristics. PVA has a low decomposition temperature so that elimination of PVA from the obtained electrospun nano-

fibre mats is an easy task.[39] Likewise, silver acetate decomposes easily by heat.[40] Accordingly, one can say that at the aforementioned calcination temperatures PVA has been completely eliminated and silver acetate decomposed into silver. The typical XRD pattern of the calcined powder at the utilised calcination temperature is presented at Figure 5. The strong and sharp diffraction peaks at 2θ values of 38.25, 44.45, 64.60 and 77.65° corresponding to the (111), (200), (220) and (311) crystal planes indicate the formation of pure crystalline silver metal (JCDPS, card no 04–0783).

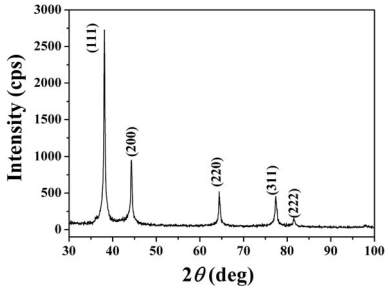

Figure 5. XRD spectra for the obtained nanofibres due to calcination of AgOAc/PVA electrospun nanofibre mats in an argon atmosphere at 700 °C.

Standard silver does have a cubic crystal structure (JCDPS, card number 04-0783). Part A of Figure 6 shows the TEM image of the obtained silver nanofibres and part B the HRTEM image. The HRTEM image draws our attention to an important observation i.e. the nanofibres are composed of attached nanoparticles and consequently the crystal planes are circular and interfere due to sintering and agglomeration of some nanoparticles as is apparent in the figure. The upper inset in Figure 6 (B) reveals the SAED pattern. The main crystal planes have been marked in the SAED image according to previous reports.[41,42] As shown in this inset, the SAED pattern reveals good crystallinity at the utilised calcination temperature. There are no dislocations or imperfections observed in the lattice planes which indicates good crystallinity of the synthesised nanofibres. The bottom inset in Figure 6 (B) demonstrates fast Fourier transform (FFT) which was invoked to obtain a clear image for calculating the planar density in the selected area.

Figure 7 (A) shows the thermogravimetric analysis for AgOAc/PVA nanofibre mats and the pristine PVA in an argon atmosphere along with a plot of the first derivative. The pristine PVA shows small decreases in the range of 100–200 °C. This decrease in the weight can be explained as evaporation of the physically bound water. Thereafter, no change in the weight was observed until about 275 °C after which the weight started to decrease rapidly until 455 °C and this decrease can be explained as due to decomposition of the polymer. It is worth mentioning that PVA did not completely eliminate since ca. 4 wt.-% was still remaining as shown in the figure. However in the case of AgOAc/PVA, the sample weight started to gradually decrease at almost 180 °C and a sharp decrease then occurred

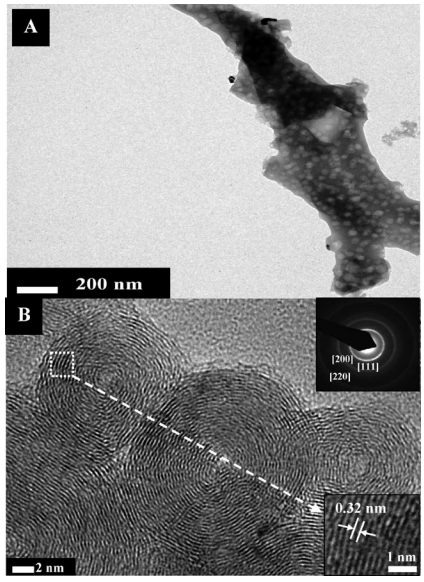

Figure 6. TEM (A) and HRTEM (B) images for silver nanofibres; the insets in image B represent SAED and FFT images.

at 340 °C and no weight change could be observed after that. A previous study on the decomposition of silver acetate in a helium atmosphere concluded that the decomposition proceeded at 170–280 °C and pure silver was obtained.[40] The mass spectrum of the gaseous products pointed to the evolution of CO, CO_2, H_2O, CH_3COOH and fragments with mass numbers 107, 216 and 275. Moreover, TGA data in that study revealed a rapid decrease in the weight at 280 °C. Accordingly, we can explain the first stage in the TGA curve of AgOAc/PVA (decreasing in the sample weight in low rate) as simultaneous decomposition of PVA and silver acetate, followed by complete decomposition of AgOAc which is responsible for the sudden decrease in the weight at 340 °C. The reducing gases obtained from the decomposition of AgOAc could be responsible for the fast elimination of the polymer compared with the pristine one. Moreover, as shown in the figure, in the case of the pristine PVA, the weight of the final residues decreased at a very small rate until the final investigation temperature. However, in the case of AgOAc/PVA, the weight was constant without any observable change in the last stage. Actually, we can explain the last finding because the remaining residues in the case of the pristine PVA slowly decompose due to the increasing temperature. However, in the case of AgOAc/PVA, the polymer completely eliminated at a relatively low temperature due to the evolved reducing gases from the acetate anion. This is considerable evidence to support the formation of pure silver from the proposed calcination process.

It is expected that the thermal decomposition behaviour of the AgOAc/PVA nanofibre mats depends on the calcination atmosphere. Figure 7 (B) shows the thermal decomposition of the prepared nanofibre mats in an *oxygen* atmosphere. As shown in this figure, the weight of the sample started to decrease rapidly at almost the same temperature

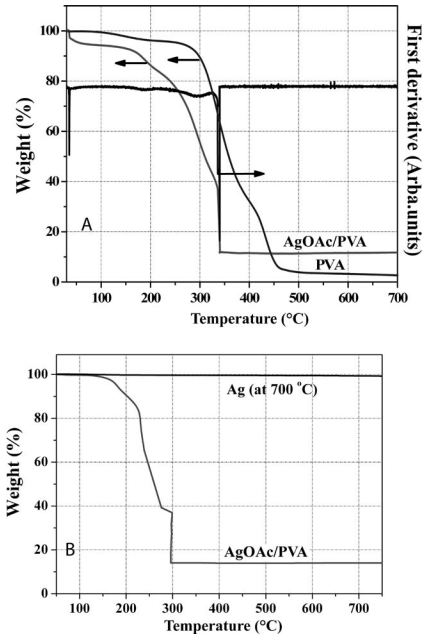

Figure 7. TGA for pristine PVA and AgOAc/PVA nanofibre mats in an argon atmosphere and the first derivative curve of the AgOAc/PVA data (A), and for AgOAc/PVA nanofibre mats and the obtained Ag nanofibres in an oxygen atmosphere (B).

as in the case of decomposition in an argon atmosphere (i.e. 180 °C). This sharp decrease in the weight finished at ca. 275 °C. Then, the weight decreased at a low rate compared with the first stage until the temperature reached to ca. 300 °C. Later, a sudden weight decrease at a constant temperature was observed followed by no further changes in the sample weight. According to the thermal properties of PVA and its mass content in the sample, we can say that PVA is completely eliminated in the first stage. This fast degradation of PVA in an oxygen atmosphere is the main problem facing researchers trying to prepare silver nanofibres.[43] Silver is an inactive metal so heating of silver acetate results in formation of silver metal. Therefore, the sudden decrease in the weight at 300 °C can be explained as decomposition of AgOAc. To ensure that the obtained nanofibres are composed of pure silver we performed TGA for the obtained silver nanofibres in an *oxygen* atmosphere. The results are demonstrated in Figure 7 (B) and, as can be observed in this curve, no weight change can be seen which indicates that the produced nanofibres consist of pure silver and this simultaneously supports the XRD and TEM results. Moreover, this finding supports the aforementioned hypothesis which states that the evolved reducing gases from AgOAc eliminate the residues left behind from the decomposition of PVA.

According to the aforementioned physiochemical characterisation results, one can say that electrospinning of a AgOAc/PVA colloidal solution was successfully achieved and that calcination of the obtained nanofibre mats results in production of pure silver nanofibres. We are suggesting Figure 8 as a conceptual illustration of the mechanism of production of silver nanofibres from the prepared colloidal solution. As presented in this diagram, after mixing silver acetate and PVA solution and because of the surface charge of the silver acetate nanoparticles indicated by the ELS analysis, the nanoparticles were dispersed in the solution due to the repulsion forces. During the electrospinning process, the AgOAc nanoparticles exit with the polymeric nanofibres and become trapped inside as shown in the illustration. After calcination, these nanoparticles decompose and attach to form silver nanofibres. The low decomposition rate of PVA as shown in the TGA results (Figure 7) gives a chance for the silver particles to bind. HR TEM results (Figure 6, B) supports this hypothesis since the crystal planes are arched and interfere which means that the nanofibres are composed of agglomerated nanoparticles.

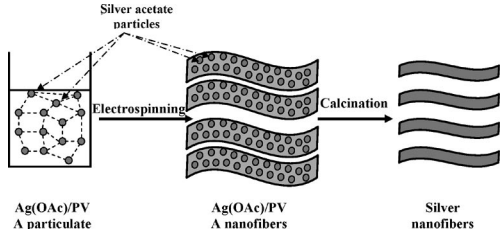

Figure 8. Illustration showing the mechanism of formation of silver nanofibres from the proposed colloidal solution.

As mentioned in the introduction section, the plasmon resonance feature strongly depends on the geometry of the nanoparticles. Many reports have been introduced discussing studies of the effect of the particle shape.[28,44,45] The main conclusion which can be drawn according to these studies is that the axial ratio does have a distinct effect. Therefore, the longer nanorods exhibit plasmon resonances in the near-infrared (near-IR) region.

Figure 9 shows the UV/Vis spectrum of the obtained sliver nanofibres. As shown in this figure, the prepared nanofibres possess surface plasmon at 962 nm which supports the previous studies affirming that increasing the axial ratios reveals SPR in the red shift side. The corresponding photon energy was 1.5 eV. These results might be interesting for researchers working in biological fields, since all the reported nanoparticles having such SPR features are alloys (e.g. gold/silver). These alloys require sophisticated procedures to prepare in a nanoparticulate shape because the nanostructure reveals that the SPR in the IR region has a special structure (e.g. core/shell). Moreover, utilising a mixture in the biological applications may be not preferable since unexpected reactions might take place with long term use. However, the introduced strategy is simple and the final product is composed of a single element with a distinct SPR. It is worth mentioning that this maximum wavelength value is not temperature dependent. Almost the same value was obtained at many silver nanofibres/water temperatures (data not shown).

Many approaches have been introduced to theoretically estimate the surface plasmon resonance. Classical electrodynamics has proven to be a valuable tool for rationalising, in

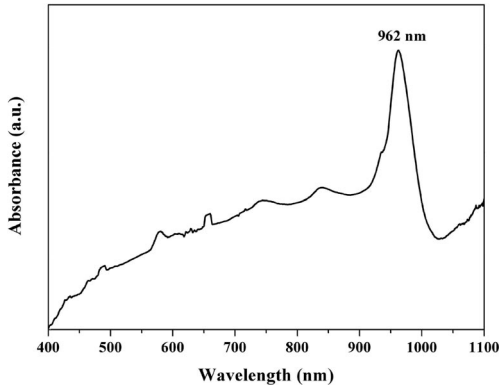

Figure 9. Surface plasmon absorption spectra of silver nanofibres.

an accurate way, the plasmon behaviour of metal nanostructures. For some simple shapes, such as spheroids, in the quasi-electrostatic regime, the resonance condition for a dipole resonance can be stated as the frequency at which the following relation is fulfilled, see Equation (1).

$$\in(\omega) = -f\in_{\mathrm{m}} \quad (1)$$

where $\in(\omega)$ stands for the complex, frequency dependent dielectric function of the particle and $\in_{\mathrm{m}}$ stands for the real part of the dielectric constant of the surrounding media (assumed to be nonabsorbing). The factor f is a geometrical factor which depends only on particle shape, i.e. the ratio of the major to minor axis (aspect ratio, R) and the incident field polarisation. This factor has been estimated for many nanostructural shapes. For instance, in the case of spheres, the f value is 2 and independent of the illumination direction. For prolate or oblate spheroids, f is greater than 2 and increases with R when the polarisation is along the major axis. Recently, Encina and Coronado[45] reported a simple graphical method to evaluate the f factor. Accordingly, the value of the f factor in the case of the produced silver nanofibres is almost 45. This value is very high and in contrast with the relative low f values found, for instance, in spherical NPs.

Electrical conductivity is an important physical feature of the nanostructure. It strongly affects using the a nanostructure in the nanodevices. Consequently, this property has been investigated for the prepared nanofibres and the thermal hysteresis phenomenon has also been studied. The latter is a phenomenon in which a physical quantity depends not only on the temperature but also on the preceding thermal history. The electrokinetic behaviour of the nanoparticle is certainly a function of temperature. Electrical conductivity is known to decrease exponentially with an increase in the interparticle spacing.[46] Therefore, the conductivity of some material nanoparticles was strongly affected by temperature, for instance gold[47] and the complex metal oxide nanoparticle In_2O_3:Sn.[48] In the case of gold nanoparticles, the conductivity changes according to the thermal hysteresis loop.[46] As gold and silver reveal almost the same behaviour in many physiochemical aspects, we have studied the thermal hysteresis of the synthesised nanofibres for the electrical conductivity and the plasmon resonance properties. A temperature range of room temperature to 90 °C was utilised. For the surface palsmon resonance, no impact was observed. However, we have found that with increasing the temperature the value of the conductivity increases and the decreases with cooling by a different path as shown in Figure 10 (A). Moreover, it is observed that the conductivity reaches a maximum and reverts to a lower value close to the initial (i.e. at 25 °C) by means of a hysteresis loop. We have built a mathematical model to represent this loop as follow, see Equation (2).

$$C = \alpha\, T^{\beta} \quad (2)$$

where C is the electric conductivity ($\mathrm{mS\,m^{-1}}$), T is the temperature (°C) and α and β are constants. The values of these constants with the mathematical accuracies are given in Table 1. To verify the validity of the designed empirical equation, the relationship between the experimental and calculated values of the electric conductivity was plotted and is represented in Figure 10 (B). As shown in this figure, all the data points are located around the forty five degree line which indicates good accuracy for the empirical model.

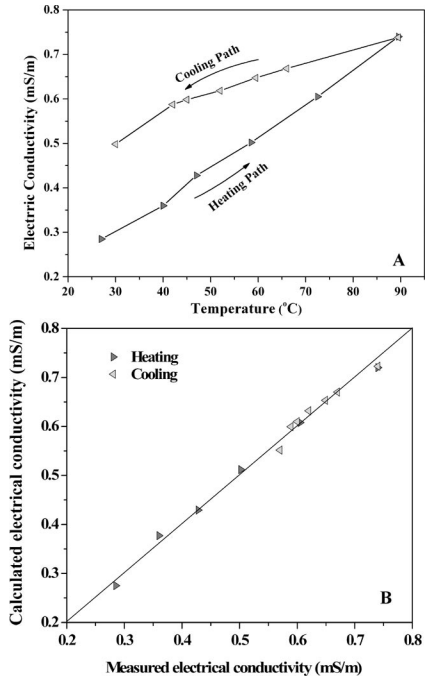

Figure 10. Thermal hysteresis by electro kinetic properties of the silver nanofibres (A) and the experimental electrical conductivity vs. the calculated ones (B).

Table 1. The empirical equation constants (α and β) in both cooling and heating paths with the correlation coefficient (R^2).

Parameter	Heating path	Cooling path	R^2
α	0.0195 ± 0.0001	0.2380 ± 0.0001	0.992
β	0.8341 ± 0.0001	0.2470 ± 0.0001	0.945

Conclusion

Addition of silver acetate to an aqueous PVA solution resulted in production of a stable colloidal solution. Electrospinning of this mixture can be carried out as a novel strategy and smooth nanofibres will be produced. The latter represents PVA nanofibres capturing AgOAc nanoparticles. Calcination of the obtained nanofibre mats in an argon atmosphere hardly changes the nanofibrous morphology and simultaneously produces pure silver nanofibres. Absence of oxygen gas from the heating environment reduces the decomposition rate of the polymer which gives a chance to the silver NPs to form silver nanofibres. The obtained nanofibres possess red-shift plasmon resonance due to the high axial ratio. The plasmon resonance occurs at a wavelength of 962 nm and it is a temperature-independent parameter. This result opens a new avenue for the silver nanofibres to be utilised in various biological fields. The electrical conductivity of the obtained nanofibres reveals thermal hysteresis behaviour. The electrical conductivity increases with an increase in temperature and does not return by the same pathway during the cooling process.

Experimental Section

Materials: Silver acetate [AgOAc, 99.9% assay] and poly(vinyl alcohol) [PVA, molecular weight (MW) = 65000 $g\,mol^{-1}$] were obtained from Showa Co., Japan and Dong Yang Chem. Co., South Korea, respectively. These materials were utilised without any further treatment. Distilled water was used as a solvent.

Experimental Work: A colloidal solution was prepared by mixing AgOAc (0.5 g) with aqueous PVA (7 g, 10 wt.-%) and stirring overnight. The obtained solution was placed in a plastic capillary. A carbon pin connected to a high-voltage generator was inserted in the solution and the solution was kept in the capillary by adjusting the inclination angle. A ground iron drum covered by a polyethylene sheet served as a counter-electrode. A voltage of 20 kV was applied to this solution. The formed nanofibre mats were initially dried for 24 h under vacuum and then calcined at 500, 700 and 850 °C for 5 h in an argon atmosphere with a heating rate of 2.3 $°C\,min^{-1}$.

Characterisation: Surface morphology was studied by using a scanning electron microscope (SEM, JSM-5900, JEOL, Japan) and a field-emission scanning electron microscope (FESEM, Hitachi S-7400, Hitachi, Japan). Hydrodynamic particles size and size distribution of the colloidal solution were determined by using a dynamic light scattering instrument (DLS) (Malvern System 4700 instrument, Otsuka Electronics Co., USA) equipped with a vertically polarised light supplied by an argon-ion laser (Cyonics) operated at 20 mW. All experiments were performed at room temperature with a measuring angle of 90° to the incident beam. The surface charge ζ-potential of the NPs was determined with an electrophoretic light scattering (ELS) instrument (ELS 8000/6000 Otsuka Electronics Co., Japan) at room temperature with a measuring angle of 20° when compared with the incident beam. Samples were sonicated in an ultra-sonic bath for one minute prior to DLS and ELS analyses. Spectroscopic characterisation was carried out by Fourier-transform infrared (FTIR), the spectra were recorded as KBr pellets using a Varian FTS 1000 FTIR, Mid-IR spectroscopic range, cooled DTGS detector from the Scimitar series, Varian Inc., Australia. Information about the phase and crystallinity was obtained by using a Rigaku X-ray diffractometer (XRD, Rigaku, Japan) with Cu-K_α (λ = 1.540 Å) radiation over Bragg angles ranging from 30 to 100°. High resolution images and selected area electron diffraction (SAED) patterns were obtained with a transmission electron microscope (TEM, JEM-2010, JEOL, Japan) operated at 200 kV. Thermal properties were studied by a thermogravimetric analyser (TGA, Pyris1, PerkinElmer Inc., USA). To study the optical and electrical conductivity properties, a colloidal solution was prepared by adding the obtained nanofibres to distilled water which was used as a blank solution to standardise the UV spectrophotometer. The mixture was sonicated for 30 min. The optical properties were studied using UV/Vis spectroscopy (HP 8453 UV Visible spectroscopy system, Germany). The spectra obtained were analysed with the HP ChemiStation software 5890 series. However, the electric conductivity was investigated using an EC meter CM 40 G Ver. 1.09 (DKK, TOA Co., Japan).

Acknowledgments

This work was supported by a grant of the Korean Ministry of Education, Science and Technology (The Regional Core Research Program/Center for Healthcare Technology & Development, Chonbuk National University, Jeonju 561-756, Republic of Korea). We thank Mr. T. S. Bae and Mr. J. C. Lim, KBSI, Jeonju branch, and Mr. Jong-Gyun Kang, Centre for University Research Facility, for taking the high-quality FESEM and TEM images.

[1] A. Formhals, US Patent, **1934**, 1,975,504.
[2] A. Formhals, US Patent, **1939**, 2,160, 962.
[3] W. Sigmund, J. Yuh, H. Park, V. Maneeratana, G. Pyrgiotakis, A. Daga, J. Taylor, J. C. Nino, *J. Am. Ceram. Soc.* **2006**, *89*, 395.
[4] D. Li, Y. Wang, Y. Xia, *Adv. Mater.* **2004**, *16*, 361.
[5] E. Smit, U. Bűttner, R. D. Sanderson, *Polymer* **2005**, *46*, 2419.
[6] I. H. Yu, S. V. Fridrikh, G. C. Rutledge, *Adv. Mater.* **2004**, *16*, 1562.
[7] D. Li, Y. Xia, *Nano Lett.* **2004**, *4*, 933.
[8] J. T. McCann, M. Marquez, Y. Xia, Z. Sun, E. Zussman, A. L. Yarin, J. H. Wendorff, A. Geirne, *Adv. Mater.* **2003**, *15*, 1929.
[9] M. Ma, V. Krikorian, J. H. Yu, E. L. Thomas, G. C. Rutledge, *Nano Lett.* **2006**, *6*, 2969.
[10] Y. Cui, Q. Q. Wei, H. Q. Park, C. M. Lieber, *Science* **2001**, *293*, 1289.
[11] D. Torres, N. Lopez, F. Illas, R. M. Lambert, *J. Am. Chem. Soc.* **2005**, *127*, 10774.
[12] M. Steffan, A. Jacob, P. Claus, H. Lang, *Catal. Commun.* **2009**, *10*, 437.
[13] P. Liu, M. Zhao, *Appl. Surf. Sci.* **2009**, *255*, 3989.
[14] A. Tao, F. Kim, C. Hess, J. Goldberger, R. R. He, Y. G. Sun, Y. N. Xia, P. D. Yang, *Nano Lett.* **2003**, *3*, 1229.
[15] C. F. Bohrem, D. R. Huffman, *Absorption and Scattering of Light by Small Particles*, Wiley-Interscience, New York, **1983**.
[16] T. Nikolajsen, T. Leosson, K. Salakutdinov, S. Bozhevolnyi, *Appl. Phys. Lett.* **2004**, *85*, 5833.
[17] C. L. Haynes, R. P. Van Duyne, *J. Phys. Chem. B* **2003**, *107*, 7426.
[18] J. H. Hodak, I. Martini, G. Hartland, *J. Phys. Chem. B* **1998**, *102*, 6985.
[19] I. H. El-Sayed, X. Huang, M. A. El-Sayed, *Nano Lett.* **2005**, *5*, 829.
[20] L. R. Hirsch, R. J. Stafford, J. A. Bankson, S. R. Sershen, B. Rivera, R. E. Price, J. D. Hazle, N. J. Halas, J. L. West, *Proc. Natl. Acad. Sci. USA* **2003**, *100*, 143549.
[21] A. D. McFarland, R. P. Van Duyne, *Nano Lett.* **2003**, *3*, 1057.
[22] L. Cognet, C. Tardin, D. Boyer, D. Choquet, P. Tamarat, B. Lounis, *Proc. Natl. Acad. Sci. USA* **2003**, *100*, 11350.

[23] J. Jiang, K. Bosnick, M. Maillard, L. Brus, *J. Phys. Chem. B* **2003**, *107*, 9964.
[24] J. A. Dionne, L. A. Sweatlock, H. A. Atwater, A. Polman, *Phys. Rev. B* **2006**, *73*, 35407-1.
[25] G. Raschke, S. Brogl, A. S. Susha, A. L. Rogach, T. A. Klar, J. Feldmann, B. Fieres, N. Petkov, T. Bein, A. Nichtl, K. Kurzinger, *Nano Lett.* **2004**, *4*, 1853.
[26] D. S. Wang, M. Kerker, *Phys. Rev. B* **1981**, *24*, 1777.
[27] B. Nikoobakht, J. Wang, M. A. El-Sayed, *Chem. Phys. Lett.* **2002**, *366*, 17.
[28] L. Kyeong-Seok, M. A. El-Sayed, *J. Phys. Chem. B* **2006**, *110*, 19220.
[29] R. Weissleder, *Nat. Biotechnol.* **2001**, *19*, 306.
[30] A. Kadir, L. Zoya, R. L. Joseph, D. G. Chris, *J. Phys. Chem. B* **2005**, *109*, 3157.
[31] H. Xin, Z. Xiujian, C. Yunxia, F. Jinyang, S. Zhenya, *J. Solid State Chem.* **2007**, *180*, 2262.
[32] J. L. Gil, I. S. Seung, C. K. Young, G. O. Seong, *Mater. Chem. Phys.* **2004**, *84*, 197.
[33] K. L. Fu, W. H. Pei, C. C. Yu, J. K. Chu, H. K. Fu, C. C. Tieh, *J. Cryst. Growth* **2005**, *273*, 439.
[34] W. Hui, Z. Rui, L. Xinxin, L. Dandan, P. Wei, *Chem. Mater.* **2007**, *19*, 3506.
[35] B. Michael, B. Mathias, G. Martin, M. Werner, H. W. Joachim, S. Andreas, W. Dirk, B. Andre, G. Armin, G. Andreas, *Adv. Mater.* **2006**, *18*, 2384.
[36] F. A. Sheikh, N. A. M. Barakat, M. Kanjwal, S. Aryal, M. S. Khil, H. Y. Kim, *J. Mater. Sci:. Mater. Med.* **2009**, *20*, 821.
[37] Y. Jiang, Y. Wu, B. Xie, Y. Xie, T. Qian, *Mater. Chem. Phys.* **2002**, *74*, 234.
[38] N. A. M. Barakat, M. S. Khil, F. A. Sheikh, H. Y. Kim, *J. Phys. Chem. C* **2008**, *112*, 12225.
[39] V. Logvinenko, O. Polunina, Y. Mikhailov, K. Mikhailov, B. Bokhonov, *J. Therm. Anal. Calorim.* **2007**, *90*, 831.
[40] D. M. Fernandes, A. A. W. Hechenleitner, E. A. G. Pineda, *Thermochim. Acta* **2006**, *441*, 101.
[41] A. Wang, H. Yin, M. Ren, Y. Liu, T. Jiang, *Appl. Surf. Sci.* **2008**, *254*, 6527.
[42] A. Graff1, D. Wagner, H. Ditlbacher, U. Kreibig, *Eur. Phys. J. D* **2005**, *34*, 263.
[43] N. A. M. Barakat, K. D. Woo, M. A. Kanjwal, K. E. Choi, M. S. Khil, H. Y. Kim, *Langmuir* **2008**, *24*, 11982.
[44] J. Benjamin, S. H. I. Wiley, Y. L. Zhi, M. Joeseph, S. Andrew, X. Younan, *J. Phys. Chem. B* **2006**, *110*, 15666.
[45] E. R. Encina, E. A. Coronado, *J. Phys. Chem. C* **2007**, *111*, 16796.
[46] T. Sarkara, S. Roy, J. Bhattacharya, D. Bhattacharya, C. K. Mitra, A. K. Dasgupt, *J. Colloid. Interface Sci.* **2008**, *327*, 224.
[47] M. N. Wybourne, L. N. Clarke, C. A. Berven, J. E. Hutchison, L. O. Brown, J. L. Mooster, *Mater. Res. Soc. Symp. Proc.* **2001**, *582*, H13.4.
[48] M. Gross, A. Winnackera, P. J. Wellmann, *Thin Solid Films* **2007**, *515*, 8567.

Received: May 19, 2009
Published Online: October 29, 2009
Publication delayed on authors' request

